Synthesis, characterization of Co1-xNixAl2O4 Spinel system and catalytic role in the synthesis of dihydropyrimidinone

Teotone Vaz
St. Xavier's College
Pranav P. Naik
St. Xavier's College https://orcid.org/0000-0002-9132-8145
Janesline Fernandes
St. Xavier's College
Lalitprabha Salgaonkar
Goa University
Snehal S. Hasolkar (19hasolkar@gmail.com)
Ganapt Parsekar College of Education

Research Article

Keywords: Lattice constant, Spinel structure, Catalytic activity, Saturation magnetization

Posted Date: June 11th, 2021

DOI: https://doi.org/10.21203/rs.3.rs-605742/v1

Abstract

In the present investigation, Spinel systems with chemical composition $Co_{1-x}Ni_xAl_2O_4$ (x = 0.0, 0.25, 0.5, and 0.75) have been successfully synthesized by the co-precipitation citrate precursor technique. The phase formation, crystal structure, and impurity check were confirmed by X-ray powdered diffraction (XRD) and Fourier transforms infrared (FTIR) spectroscopy technique. The particle size estimation was done using a transmission electron microscope (TEM). Investigation of magnetic behavior and parameters such as saturation magnetization (M_S), coercivity (H_R), and retentivity (M_R) was done using a vibrating sample magnetometer (VSM). The catalytic activity of prepared spinel systems was explored for the one-pot synthesis of dihydropyrimidinone derivatives. The catalytic product was identified by comparison of melting point and the spectral data (FTIR).

Highlights

The highlights of the research work presented are as follows

- Synthesis of $Co_{1-x}Ni_xAl_2O_4$ via co-precipitation citrate precursor technique
- Particle size distribution was seen to be very narrow.
- Ni^{+2} concentration dependent lattice constant variation was observed.
- Variation in Magnetic properties was seen with increasing Ni^{+2} Concentration
- Increase in percentage yield of dihydropyrimidinone in presence of $Co_{1-x}Ni_xAl_2O_4$

1 Introduction

The nanostructured cobalt aluminate spinels have been the center of attraction due to their unique electrical, magnetic, optical, and catalytic properties. These materials find their application in the field of high-density magnetic recording, microwave devices, applications such as plastics coloring and glass coatings, etc. [1-5,6,7]. The unusual magnetic behavior of FCC structure resulting from geometrical frustration makes it a system of great importance as it is an exemplary system possessing degenerate frustrated ground states which are the result of competition between various exchange interactions and further lead to spin-liquid behavior[8-10]. The spinel composition $CoAl_2O_4$ is also known for its catalytic properties arising from high surface area and optimum basicity of the spinel structure and hence have been the subject of an investigation to explore their potential catalytic applications for organic synthesis[11-14]. Studies have shown that these spinel oxides are better catalysts on account of their activity and stability. The phenomenon of synergism in two or three metal-based catalysts is a fascinating aspect of catalytic research [15].

Researchers have synthesized cobalt aluminates using several methods such as microwave combustion method, low-temperature combustion method, sol-gel process, hydrothermal method, reverse microemulsion process, sonochemical process, polymeric-aerosol pyrolysis, freeze-drying, ultrasonic-

assisted-hydrothermal method, chemical vapor deposition (CVD) technique, polymerized complex technique, etc. It has been observed that the properties of resultant cobalt aluminate products are also administered by the method of preparation [16].

In this report the synthesis and characterization of Ni substituted cobalt aluminate nano-powders with compositions $CoAl_2O_4$, $Co_{0.75}Ni_{0.25}Al_2O_4$, $Co_{0.5}Ni_{0.5}Al_2O_4$, and $Co_{0.25}Ni_{0.75}Al_2O_4$ using co-precipitation precursor technique using citrate solution has been reported. The report also includes the investigation of the catalytic efficiency effect of Ni^{+2} substituted cobalt aluminate in synthesizing dihydropyrimidinone via Bignelli reaction.

2. Experimental

2.1 Co-precipitation precursor synthesis

The Spinel structured $Co_{1-x}Ni_xAl_2O_4$ (x=0.0,0.25, 0.50, and 0.75) nanocrystalline compositions were synthesized by co-precipitation precursor technique using Citrate solution [17,18]. Stoichiometric quantities of hydrated AR grade reagents $Co(NO_3)_3$, $Ni(NO_3)_3$, $Al(NO_3)_3$ were dissolved in 100mL of double-distilled water in a beaker labeled as 'A'. In another beaker labeled as 'B, an equimolar amount of citric acid was dissolved separately in double-distilled water. The citrate solution from beaker B was added dropwise to the solution in beaker A and continuously stirred on a magnetic stirrer for 2 hours with the temperature maintained at 60°C. The temperature was raised further to initiate slow evaporation and reduce the quantity to half, leading to the setting of the desirable gel. The gel thus obtained was subjected to an overnight and slow decomposition process at an elevated temperature of 200°C. The fluffy mass obtained at the end of decomposition was then subjected to heat treatment at 300°C to eliminate the carbonaceous matter. The dried powder was ball milled for 4 hours to attain uniformity in particle size. The processed powders were further heated at finally 800°C in the air for a total time of 10 hours, and were furnace cooled, and stored in airtight containers for characterization. The process of material preparation is as shown in Figure 1.

2.2 Characterization of as-synthesized materials:

The prepared materials were characterized by X-ray powder diffraction technique with Rigaku Miniflex benchtop instrument, using Cu Kα, filtered through Ni absorber. FTIR spectra were recorded on a Shimadzu FTIR instrument (model 8101A) in the range of 4000 - 500 cm^{-1}. The transmission electron micrographs were obtained on a Hitachi 200kV Transmission electron microscope (S.A.I.F., IIT Bombay). The magnetic hysteresis loops for $Co_{1-x}Ni_xAl_2O_4$ nanocrystalline powders were recorded on Quantum design's 3T vibrating sample magnetometer.

3 Results And Discussion

3.1 X-ray diffraction analysis

The prepared compositions were characterized by X-ray powder diffraction. The X-ray diffraction patterns were recorded at room temperature with a 2θ scanning angle ranging from 20° to 70°.

Figure 2 shows the Rietveld refinement of the XRD pattern for the $Co_{1-X}Ni_XAl_2O_4$ (x = 0.0, 0.25, 0.50, and 0.75) system performed using Fullprof software. The major Bragg reflections were seen at 2θ values of 31.25, 36.14, 38..36, 44.20, 55.92, and 65.51 corresponding to corresponding to the [220], [311], [400], [422], [511] and [440] diffraction planes and were seen to be in accordance with JCPDS data file **44-0160** indicating the formation of pure spinel phase belonging to Fd3m space group without any impurity [19,20]. The goodness of refinement quality is evident from the refinement parameters (c2, R_{wp}, R_{exp}, RBragg, and RF) listed in table 1.

Table 1 Refinement parameters obtained Rietveld analysis

Material composition	c^2	R_{WP}	R_{EXP}	R_{BRAGG}	$R_{F\text{-}FACTOR}$
$CoAl_2O_4$	1.38	81	68.7	57.3	39.3
$Co_{0.75}Ni_{0.25}Al_2O_4$	1.42	54.2	45.4	17.4	14.3
$Co_{0.50}Ni_{0.50}Al_2O_4$	1.24	57.5	51.7	27.9	20.6
$Co_{0.25}Ni_{0.75}Al_2O_4$	1.59	83.2	65.8	63.2	44.2

The variation of lattice constant '*a*', x-ray density, and cell volume as a function of Ni^{+2} concentration are shown in Figure 3 (a,b) The lattice constant was seen to decrease initially for x=0.0 to x=0.25 and further showed a marginal rise with increasing Ni^{+2} at the tetrahedral site. The initial decrease in lattice constant can be attributed to smaller ionic radii of Ni^{+2} ions (0.83Å) replacing the larger Co^{+2} ions with ionic radii of 0.88Å [21]. For the compositions beyond x=0.25 i.e. for x=0.50 and 0.75, the increase in lattice constant could be due to electrostatic shielding caused by 3d electrons of Ni^{+2} ions diluting the nuclear dominance and causing marginal expansion in the tetrahedral environment [22]. A trend similar to that of lattice constant variation was observed in the values of cell volume while x-ray density was seen to vary inversely (Figure 2b).

3.2 FTIR spectra analysis

Figure 4 shows IR absorption bands for citrate precursor and $Co_{1-X}Ni_XAl_2O_4$ system, in the range of 4000-500 cm^{-1}. In general, FTIR spectra of all the prepared spinels show weak absorption bands at about 3450, 1630, and 1385 cm^{-1}. The characteristic vibrational frequencies of $CoAl_2O_4$ aluminate spinel appeared in the range of 750-400 cm^{-1}. The absorption band around 3400 to 3500 cm-1 was assigned to stretching vibrations and 160-1400cm-1 is assigned to bending vibration respectively which is due to adsorbed moisture. The band observed at 750-500 cm^{-1} can be attributed to the symmetric stretching (ν_1), bending (ν_2), and asymmetric stretching (ν_3) modes of M-O-Al, M-O, and Al-O bonds at tetrahedral and octahedral sites in $CoAl_2O_4$ lattice [23]. The broad absorption bands observed at 670 and 560 cm^{-1} are the characteristic vibrational bands representing a typical pattern of $CoAl_2O_4$ normal spinel structure, in

agreement with the literature [24]. These bands correspond to the AlO_6 units, which is the mainframe of the $CoAl_2O_4$ crystal, and ensure the formation of spinel structure. The absorption frequencies observed between 1800-1000 cm^{-1} were assigned to the deformation mode of Al-OH and Co-OH, which is typical of this class of materials [25]. In the $Co_{0.25}Ni_{0.75}Al_2O_4$ nanoparticle spectra (e), the prominent vibrational peaks observed at around 600, 530, and 495 cm^{-1}, the absence of a strong absorption band at 560 $cm^{-1,}$ and the appearance of a stronger frequency band at around 598 cm^{-1} indicate the substitution of Ni atoms has taken place replacing Co atoms in the lattice. The first two absorption peaks are attributed to the intrinsic stretching vibrations of the M-O at tetrahedral sites, while the lower mode is assigned to the stretching vibration of the M-O at the octahedral site[23-27]. No other impurity or organic matter absorption bands were observed indicating the purity of the materials, in agreement with the results obtained by XRD. FTIR measurements were also helpful to illustrate the formation of spinel from the precursor.

3.3 VSM data analysis

The magnetic hysteresis loops obtained at room temperature for $Co_{1-x}Ni_xAl_2O_4$ nano-powders are shown in Figure 5

The samples were seen to exhibit paramagnetic behavior [1]. The values of saturation magnetization (M_S), coercive field (H_C), and remnant magnetization (M_R) are listed in Table 3.

Table 3 Values of magnetic parameters obtained for $Co_{1-x}Ni_xAl_2O_4$

Sample	Saturation Magnetization (M_S) emu/g	Coercive field (H_C) Oe	Remnant Magnetization (H_R) emu/g	Squareness	Magnetic Moment m (Bohr Magneton)
$CoAl_2O_4$	0.56	16.04	0.05	0.083	0.018
$Co_{0.75}Ni_{0.25}Al_2O_4$	0.51	24.06	0.03	0.058	0.016
$Co_{0.50}Ni_{0.50}Al_2O_4$	0.72	72.18	0.04	0.061	0.022
$Co_{0.25}Ni_{0.75}Al_2O_4$	0.66	24.34	0.04	0.051	0.020

The M_S values were seen to vary with Ni^{+2} content and showed a maximum value of 0.72emu/g for x=0.5 and a minimum of 0.51emu/g for x=0.25 while the remnant magnetization was seen to remain almost constant with values ranging between 0.03emu/g to 0.05emu/g. The squareness values calculated using the following equation (1) were found to be very low confirming the paramagnetic behavior of the nano-powders. However, these values were much higher than the reported squareness limit for superparamagnetic materials [28-30]. The magnetic moment m calculated for all the samples using equation (2) was seen to remain in the range of 0.016 to 0.022 Bohr magneton with increasing Ni concentration in the spinel lattice [31-35].

$$Squareness = \frac{M_R}{M_S}$$ Equation 1

$$\mu = \frac{M_S M_X}{5585}$$ Equation 2

Where Mx is the molecular weight of the composition.

The anisotropy constant was calculated using equation 3 given below showed a trend similar to that of HC. The plot of variation in anisotropy constant 'K' with increasing Ni concentration is shown in figure 6.

$$K = M_S H_C / 0.96$$ Equation 3

3.4 TEM image analysis

The transmission electron micrographs obtained on $CoAl_2O_4$ and $Co_{0.25}Ni_{0.75}Al2O_4$ nanocrystalline powders along with particle size distribution histograms are shown in Figure 7. The observed particle size of these nanocrystalline spinel aluminates was in the range of 20 nm to 47 nm.

3.5 The Bignelli reaction as a model catalytic application

The as-synthesized spinel Co-Ni aluminate compositions were explored for catalytic efficiency of synthesizing dihydropyrimidinone derivative as a model test reaction as shown in Figure 8. A solution of Benzaldehyde (10 mmol, 1.06 g), ethylaceto acetate (13mmol, 1.69 g), and urea (15 mmol, 0.90g) was refluxed at 85-90°C in ethanol in the presence of materials (0.2g) under investigation, for 3 hours. On completion of the reaction, the catalyst was filtered off from the mixture, and the filtrate was collected in crushed ice. The product obtained was recrystallized using ethyl acetate. The synthesized product was identified by comparison of melting point (mp) and the spectral data (FTIR).

The catalytic product was confirmed by melting point (mp) and FTIR spectroscopy. Table 4 summarises the yield obtained (%) for the dihydropyrimidinone product. The results obtained using Ni substituted cobalt ferrite nanopowders as catalyst are comparable to those obtained by Ezzat Rafiee et. al. in which dihydropyrimidinone was reported to synthesize using heteropoly acids such as $H_3PW_{12}O_{40}$, $H_3PMo_{12}O_{40}$ [35]. The efficiency nanopowders of $Co_{1-X}Ni_XAl_2O_4$ can be enhanced to produce higher yield by increasing the Ni concentration in the composition as these nanopowders possess higher surface area in comparison to that of heteropoly acids.

Table 4 Yield of dihydropyrimidinone and their melting points.

Nanocatalysts	% Yield	Physical constant (mp)
In the absence of a catalyst	30%	207°C
$CoAl_2O_4$	45.91%	205°C
$Co_{0.75}Ni_{0.25}Al_2O_4$	46.34%	205°C
$Co_{0.50}Ni_{0.50}Al_2O_4$	49.79%	207°C
$Co_{0.25}Ni_{0.75}Al_2O_4$	51.93%	206°C

Figure 9 shows the FTIR spectra of the product and the characteristic absorbance peaks which are summarised in Table.5, confirming the formation and purity of dihydropyrimidinone The melting point of the purified product was found to be ranging between 205^{o}C to 207 ^{O}C which again indicated the purity of the reaction product [36-40].

Table 5 Characteristic absorption peaks of dihydropyrimidinone.

Observed absorption bands (cm^{-1})	Type of stretching
3337.39	N-H stretch
3115.53	N-H stretch
2979.46	C-H stretch
1725.29	C=O ester stretch
1702.88	C=O amide stretch
1650.29	C=C stretch
1089.21	Monosubstituted aromatic ring

As the atomic concentration of Al remains practically the same in all the $Co_{1-x}Ni_xAl_2O_4$ spinel nanomaterials, it may have an indirect role in the activity. The observed increase of 30 to 51 % in the yield percentage with the Ni substitution and its atomic concentration in $CoAl_2O_4$ crystal structure, may be attributed due to atomic size variation and synergistic effect of both Co^{+2} and Ni^{+2} ions.

4 Conclusion

Nanocrystalline powders of Ni^{+2} substituted Cobalt aluminate with chemical composition $Co_{1-x}Ni_xAl_2O_4$ (x=0.0, 0.25, 0.5, 0.75) were successfully prepared by co-precipitation precursor technique using citrate solution. Samples were seen to exhibit pure spinel phase and particle size ranging between 25 nm to 40 nm. Structural parameters such as lattice constant, cell volume, and X-ray density were seen to change with varying Ni^{+2} concentrations.

The FTIR spectra confirmed the existence of characteristic spinel bands confirming the phase purity. All the samples exhibit paramagnetic behavior with saturation magnetization varying between 0.7 to 0.5 emu/g. The application of $Co_{1-x}Ni_xAl_2O_4$ nanopowders as a catalyst in the synthesis of dihydropyrimidinone was investigated. The reaction showed an enhancement of 15 percent in percentage yield with pure $CoAl_2O_4$ employed as catalyst. The percentage yield was seen to increase further by 21

percent with increasing Ni content in the spinel structure. The efficiency of $Co_{1-x}Ni_xAl_2O_4$ can be improved further by increasing Ni concentration and can be used as more efficient catalyst due to its larger surface area.

Declarations

We the authors of the manuscript entitled "**Synthesis, characterization of $Co_{1-x}Ni_xAl_2O_4$ Spinel system and catalytic applications in the synthesis of dihydropyrimidinone**" declare that

1. The article is original.
2. The article has been written by the stated authors who are all aware of its content and approve its submission.
3. The article has not been published previously
4. The article is not under consideration for publication elsewhere
5. No conflict of interest exists, or if such conflict exists, the exact nature must be declared.

If accepted, the article will not be published elsewhere in the same form, in any language, without the written content of the publisher.

The present work entitled Synthesis, characterization of $Co_{1-x}Ni_xAl_2O_4$ Spinel system and catalytic applications in the synthesis of dihydropyrimidinone includes the synthesis and characterization of Ni substituted cobalt aluminate nano-powders with compositions $CoAl_2O_4$, $Co_{0.75}Ni_{0.25}Al_2O_4$, $Co_{0.5}Ni_{0.5}Al_2O_4$, and $Co_{0.25}Ni_{0.75}Al_2O_4$ using co-precipitation precursor technique using citrate solution. The report also includes the investigation of the catalytic efficiency effect of Ni^{+2} substituted cobalt aluminate in synthesizing dihydropyrimidinone via Bignelli reaction.

References

1. Mohamed Karmaoui, Nuno J. O. Silva, Vitor S. Amaral, Alfonso Ibarra, Angel Millan, Fernando Palacio, Synthesis of cobalt aluminate nano pigments by a non-aqueous sol-gel route, Nanoscale, 2013, DOI: 10.1039/c3nr34229h.
2. J. Merikhi, H.-O. Jungk and C. Feldmann, Sub-micrometer CoAl2O4 pigment particles Ð synthesis and preparation of coatings, J. Mater. Chem., 2000, 10, 1311–1314
3. C. Feldmann, Preparation of Nanoscale Pigment Particles, Adv. Mater., 2001, 13, 1301-1303.
4. Assunta Campanile, Barbara Liguori, Ottavio Marino, GennaroCavaliere, Valter Luca De Bartolomeis, Domenico Caputo, Facile synthesis of nanostructured cobalt pigments by Co- A zeolite thermal conversion and its application in porcelain manufacture, Scientific Reports, 2020, DOI: 10.1038/s41598-020-67282-1
5. A. A. Ali, E. El Fadaly, I. S. Ahmed, Near-infrared reflecting blue inorganic nano-pigment based on cobalt aluminate spinel via combustion synthesis method. Dye. Pigment.,

https://doi.org/10.1016/j.dyepig.2018.05.058 (2018).

6. J. L. Dormann, M. Seqqat, D. Fiorani, M. Nogu`es, J. Soubeyroux, S. Bhargava, P. Renaudin, Mössbauer studies of $FeAl_2O_4$ and $FeIn_2S_4$ spin glass spinels, Hyperfine Interact., 1990, 54, 503–507.
7. Ritu Malik, Vijay K. Tomar, State-of-the art review of morphological advancements in graphite carbon nitride (g-CN) for sustainable hydrogen production, Renewable and Sustainable Energy Reviews, 2021, 135, 110235
8. Ritu Malik, Vijay K. Tomer, Yogendra Kumar Mishra, Liwei Lin, Functional gas sensing nanomaterials: A panoramic view, Applied Physics Reviews 7, 021301 (2020), DOI:10.1063/1.5123479
9. W. L. Roth, Magnetic properties of normal spinels with only a-a interactions, J. Phys., 1964, 25, 507–515.
10. J. L. Soubeyroux, D. Fiorani, E. Agostinelli, S. C. Bhargava and J. L. Dormann, Spin glass behaviour in iron spinels, J. Phys., 1988, 49, C8-1117.
11. W. Xu, X. Liu, J. Ren, P. Zhang, Y. Wang, Y. Guo, Y. Guo and G. Lu, Catalytic conversion of biomass-derived carbohydrates into fuels and chemicals via furanic aldehydes, Catal. Commun., 2010, 11, 721–726.
12. W. Xu, H. Wang, X. Liu, J. Ren, Y. Wang and G. Lu, Direct catalytic conversion of furfural to 1,5-pentanediol by hydrogenolysis of the furan ring under mild conditions over Pt/Co2AlO4 catalyst, Chem. Commun., 2011, 47, 3924–3926.
13. Christine Azer, Adham R. Ramadan, Gehane Ghaly, Jehane Ragai, Preparation and Characterization of Cobalt Aluminate Spinels CoAl2O4 Doped with Magnesium Oxide, Adsorption Science & Technology, 2012, Vol. 30 No. 5, 399-407
14. A. Dandapat and G. De, ACS Appl. Mater. Interfaces, Host-Mediated Synthesis of Cobalt Aluminate/γ-Alumina Nanoflakes: A Dispersible Composite Pigment with High Catalytic Activities, 2012, 4, 228–234.
15. V. Manikandan, Iulian Petrila, S. Vigneselvan, R. S. Mane, d Bogdan Vasile, Raghu Dharmavarapu, Stefan Lundgaard, Saulius Juodkazis and J. Chandrasekaran, A reliable chemiresistive sensor of nickel-doped tin oxide (Ni-SnO2) for sensing carbon dioxide gas and humidity, RSC Adv., 2020, 10, 3796–3804.
16. Ederson Rossi Abaide, Chayene Gonçalves Anchieta, Vitória Segabinazzi Foletto, Beatriz Reinehr, Lucielle Ferreira Nunes, Raquel Cristine Kuhn, Marcio Antonio Mazutti, Edson Luiz Foletto, Production of Copper and Cobalt Aluminate Spinels and Their Application As Supports for Inulinase Immobilization, Materials Research. 2015; 18(5): 1062-1069
17. Saeid Khademolhoseini, Ruhollah Talebi, Green synthesis and characterization of cobalt aluminate nanoparticles and its photocatalyst application, J Mater Sci: Mater Electron (2016) 27:2938–2943
18. M. Maddahfar, M. Ramezani, M. Sadeghi, A. Sobhani-Nasab, $NiAl_2O_4$ nanoparticles: synthesis and characterization through modified sol-gel method and its photocatalyst applications, J. of Mater. Sc.: Materials in Electronics 26:10 (2015) 7745-7750

19. Guido Busca, Vincenzo Lorenzelli, Vera Bolis, Preparation, bulk characterization and surface chemistry of high-surface-area cobalt aluminate, Materials Chemistry and Physics, Volume 31, Issue 3, May 1992, Pages 221-228
20. C. Ragupathi, J. Judith Vijaya, L. John Kennedy, Preparation, characterization and catalyticproperties of nickel aluminate nanoparticles:A comparison between conventional andmicrowave method, Journal of Saudi Chemical Society Volume 21, Supplement 1, January 2017, Pages 231-239
21. Z. Chen, E. Shi, W. Li, Y. Zheng, N. Wu, W. Zhong, Particle size comparison of hydrothermally synthesized cobalt and zinc aluminate spinels, J. Am. Ceram. Soc. 85 (2002) 2949–2955.
22. Brian T. Naughton and David R. Clarke, Lattice Expansion and Saturation Magnetization of Nickel–Zinc Ferrite Nanoparticles Prepared by Aqueous Precipitation, J. Am. Ceram. Soc., 90 (2007) [11] 3541–3546
23. M. Zayat, D. Levy, Blue $CoAl_2O_4$ particles prepared by the sol-gel and citrate-gel methods, Chem. Mater. 12 (2000) 2763-2769
24. T. Tangcharoen, J. T-Thienprasert, C. Kongmark, Optical properties and versatile photocatalytic degradation ability of MAl_2O_4 (M = Ni, Cu, Zn) aluminate spinel nanoparticles, J. Mater. Sc.: Materials in Electronics, 2018, DOI: 10.1007/s10854-018-8924-4
25. S.C. Laha, P. Mukherjee, S.R. Sainkar, R. Kumar, Cerium containing MCM-41-type mesoporous materials and their acidic and redox catalytic properties, J. Catal. 207 (2002) 213– 223.
26. P. Laokul, V. Amornkitbamrung, S. Seraphin, S. Maensiri, Characterization and magnetic properties of nanocrystalline CuFe2O4, NiFe2O4, ZnFe2O4 powders prepared by the aloe vera extract solution, Curr. Appl Phys. 11 (2011) 101–108.
27. F. Meyer, R. Hempelmann, S. Mathurband, M. Veith, Microemulsion mediated sol–gel synthesis of nano-scaled MAl2O4 (M,Co, Ni, Cu) spinels from single-source heterobimetallic alkoxide precursors, J. Mater. Chem. 9 (1999) 1755–1763.
28. Pranav P Naik, RB Tangsali, SS Meena, SM Yusuf, Influence of rare earth (Nd+3) doping on structural and magnetic properties of nanocrystalline manganese-zinc ferrite, Materials Chemistry and Physics, 191, (2017), 215-224.
29. Pranav P Naik, Snehal S Hasolkar, Manoj M Kothawale, Satish HP Keluskar, Altering saturation magnetization of manganese zinc ferrite nanoparticles by doping with rare earth Nd+3 ions, Physica B: Condensed Matter, Volume 584, (2020), 412111.
30. Snehal S Hasolkar, Pranav P Naik, Effect of Gd+3 doping on structural, magnetic and electrical properties of Mn0.5Co0.5Fe2-xGdxO4 nano-particles prepared using combustion synthesis, Journal of Alloys and Compounds, Volume 823, 2020, 153605
31. Snehal S. Hasolkar Pranav P. Naik, Consequence of B-site substitution of rare earth (Gd+3) on electrical properties of manganese ferrite nanoparticles, Journal of Materials Science: Materials in Electronics, 31, (2020) 13434–13446
32. Anuja B Naik, Pranav P Naik, Snehal S Hasolkar, Diksha Naik, Structural, magnetic and electrical properties along with antifungal activity & adsorption ability of cobalt doped manganese ferrite

nanoparticles synthesized using combustion route, Ceramics International, Volume 46, Issue 13, (2020), 21046-21055

33. Nirav Joshi, Luís F da Silva, Harsharaj S Jadhav, Flavio M Shimizu, Pedro H Suman, Jean-Claude M'Peko, Marcelo Ornaghi Orlandi, Jeong Gil Seo, Valmor R Mastelaro, Osvaldo N Oliveira Jr, Yolk-shelled $ZnCo_2O_4$ microspheres: Surface properties and gas sensing application, Sensors and Actuators B: Chemical, 257 (2018) 906-915.
34. Nirav Joshi, Luis F da Silva, Harsharaj Jadhav, Jean-Claude M'Peko, Bruno Bassi Millan Torres, Khalifa Aguir, Valmor R Mastelaro, Osvaldo N Oliveira, One-step approach for preparing ozone gas sensors based on hierarchical NiCo2O4 structures, RSC advances, 6 (2016) 92655-92662.
35. Ezzat Rafiee, Hadi Jafari, A practical and green approach towards synthesis of dihydropyrimidinones: Using heteropoly acids as efficient catalysts, Bioorganic & Medicinal Chemistry Letters 16 (2006) 2463–2466.
36. Qu H., Li X., Mo F. Lin X. Efficient synthesis of dihydropyrimidinones via a three-component Biginelli type reaction of urea, alkylaldehyde and arylaldehyde. Beilstein J. Org. Chem., (2013), 9(1), 2846–2851.
37. Peng J. and Deng Y. (2001). Ionic liquids catalyzed Biginelli reaction under solvent-free Conditions. Tetrahedron Letters, 42(34), 5917–5919.
38. Oliver Kappe C. (2000). Recent Advances in the Biginelli Dihydropyrimidine Synthesis. New Tricks from an Old Dog. Acc. Chem. Res., 33(12), 879-888.
39. P. K. Sahu, J. Lal, D. Thavaselvam , D. D. Agarwal, A facile green synthesis and in vitro antimicrobial activity 4H-pyrimido [2,1-b] [1,3] benzothiazole derivatives using aluminum trichloride under solvent free conditions, Medicinal Chemistry Research, (2012),21(11), 3826–3834.
40. A. Vasconcelos, P. S. Oliveira, M. Ritter, R. A. Freitag, R. L. Romano, F. Quina, L. Pizzuti, C. Pereira, M. S. Francieli. G. B. Alethéa, Antioxidant capacity and environmentally friendly synthesis of dihydropyrimidin- (2H)-ones promoted by naturally occurring organic acids. Journal of Biochemical and Molecular Toxicology, 2012, 26(4), 155-161.

Figures

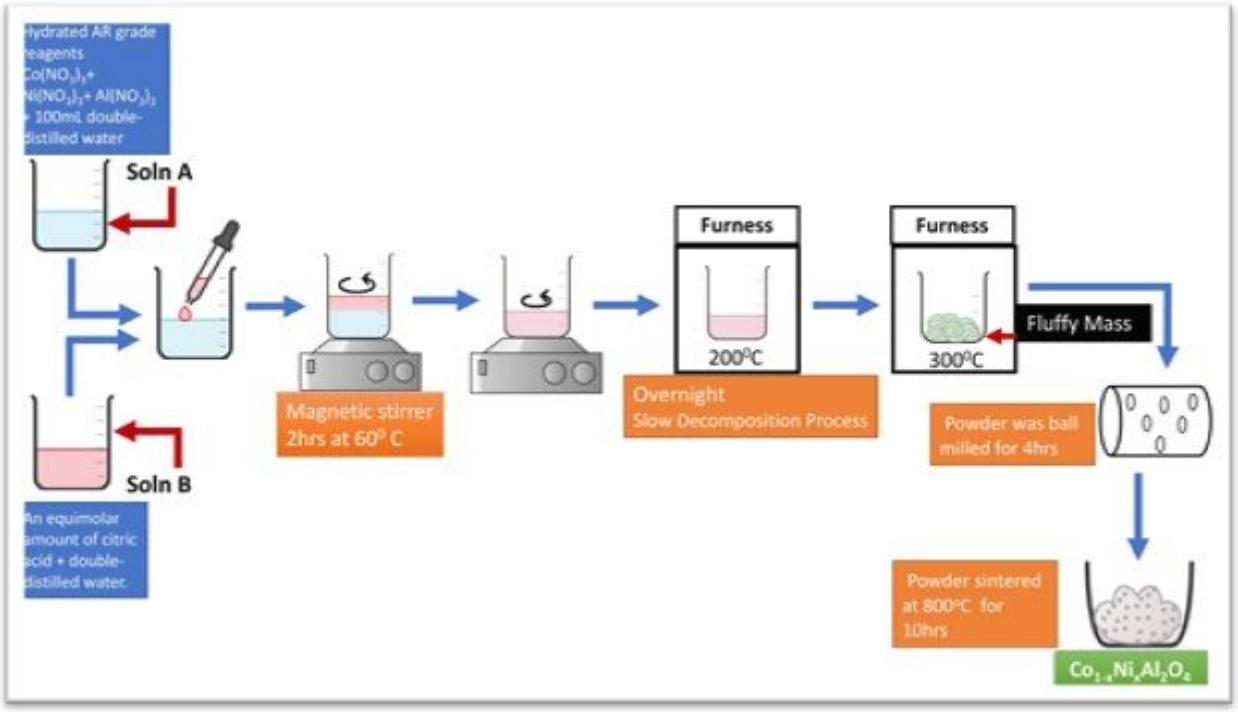

Figure 1

Co-precipitation precursor technique using Citrate solution

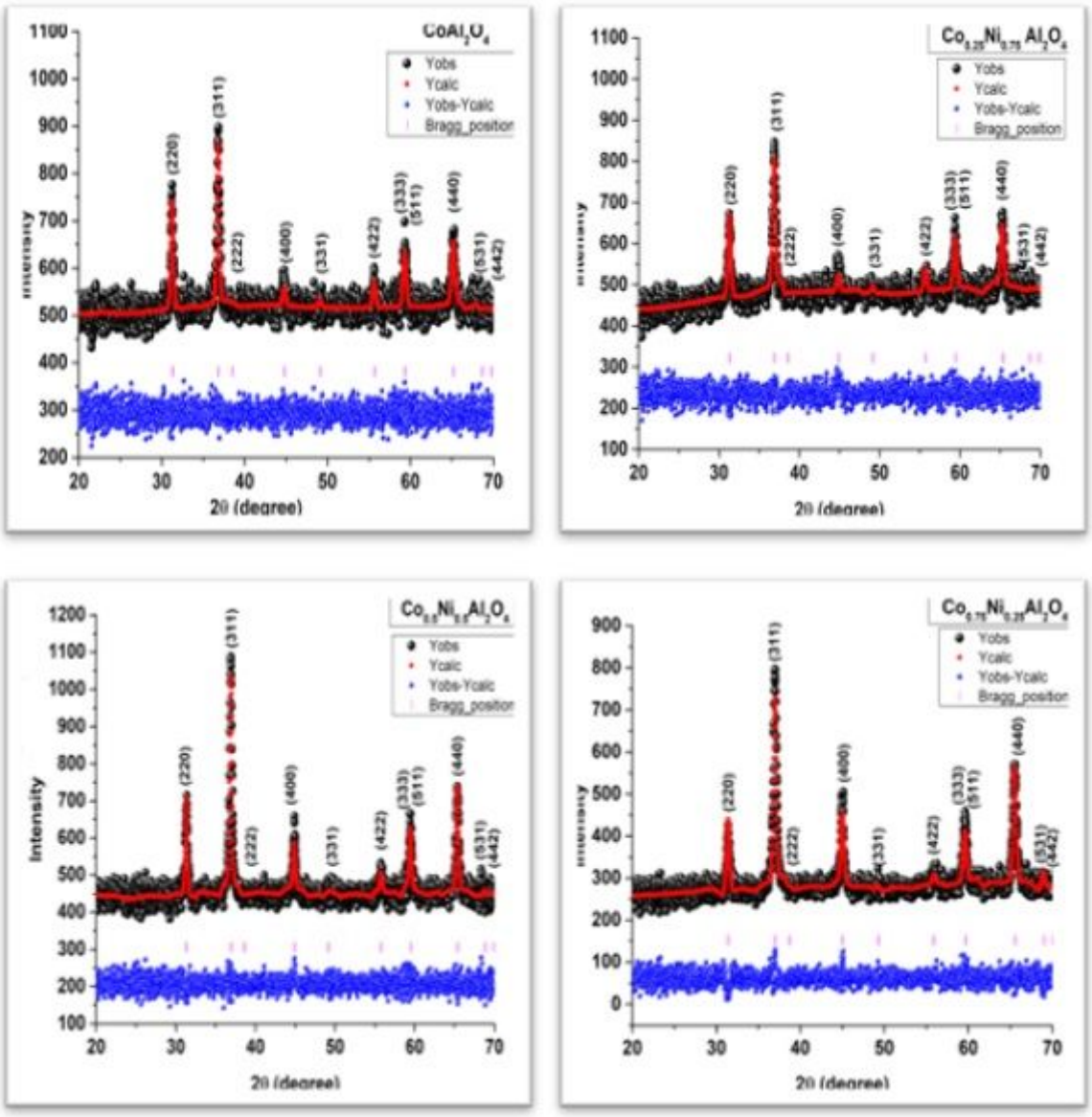

Figure 2

Rietveld refinement of XRD patterns obtained for Co1-xNixAl2O4

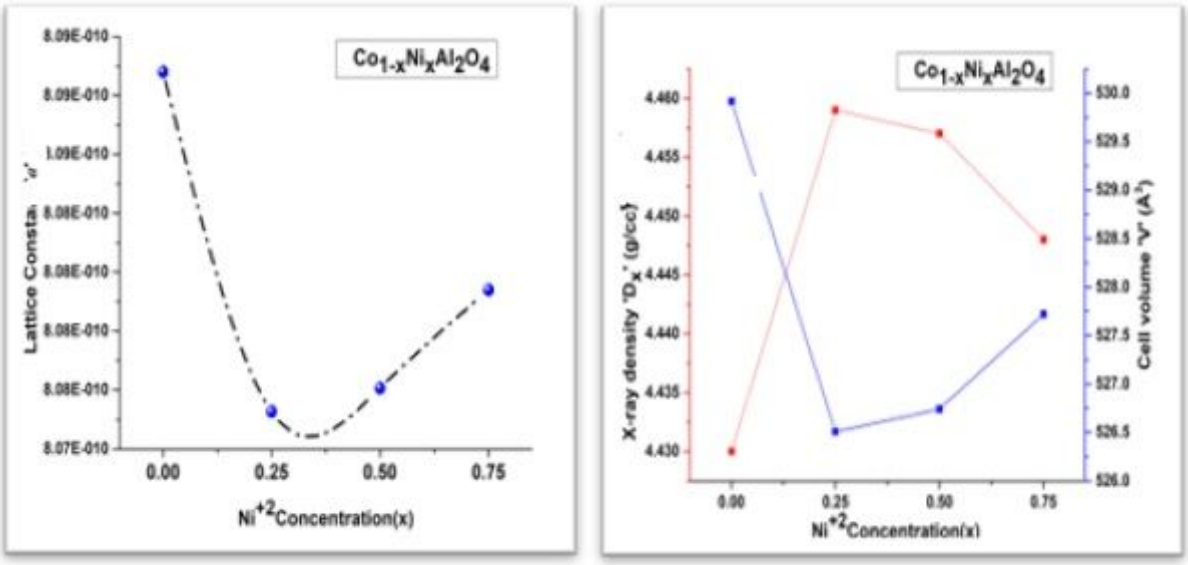

Figure 3

Variation of (a) Lattice constant and (b) X-ray density, cell volume with Ni+2 concentration

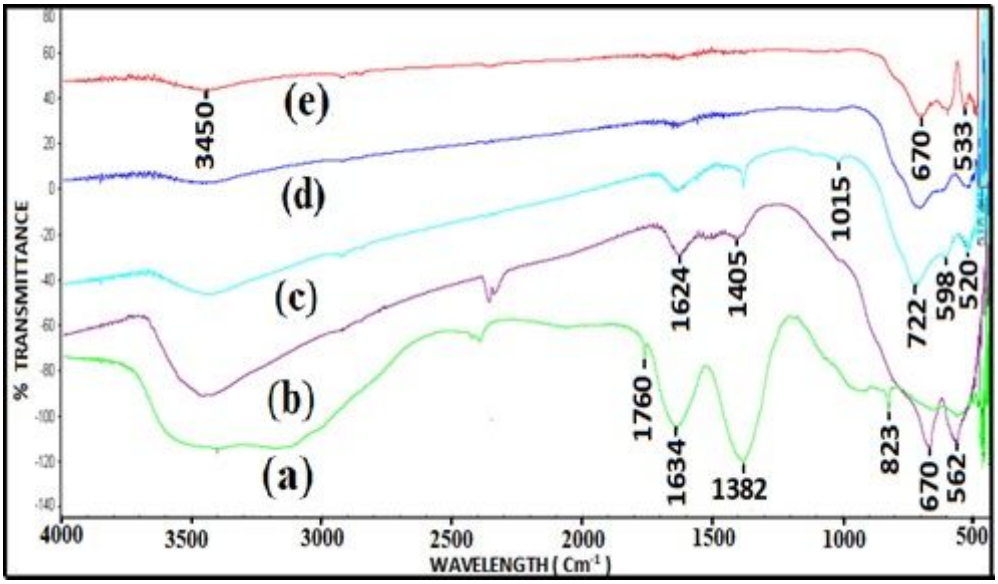

Figure 4

FTIR spectra of (a) Cobalt Nickel Citrate Precursor (b) CoAl2O4 (c) Co0.75Ni0.25Al2O4 (d) Co0.5Ni0.5Al2O4, and (e) Co0.25Ni0.75Al2O4.

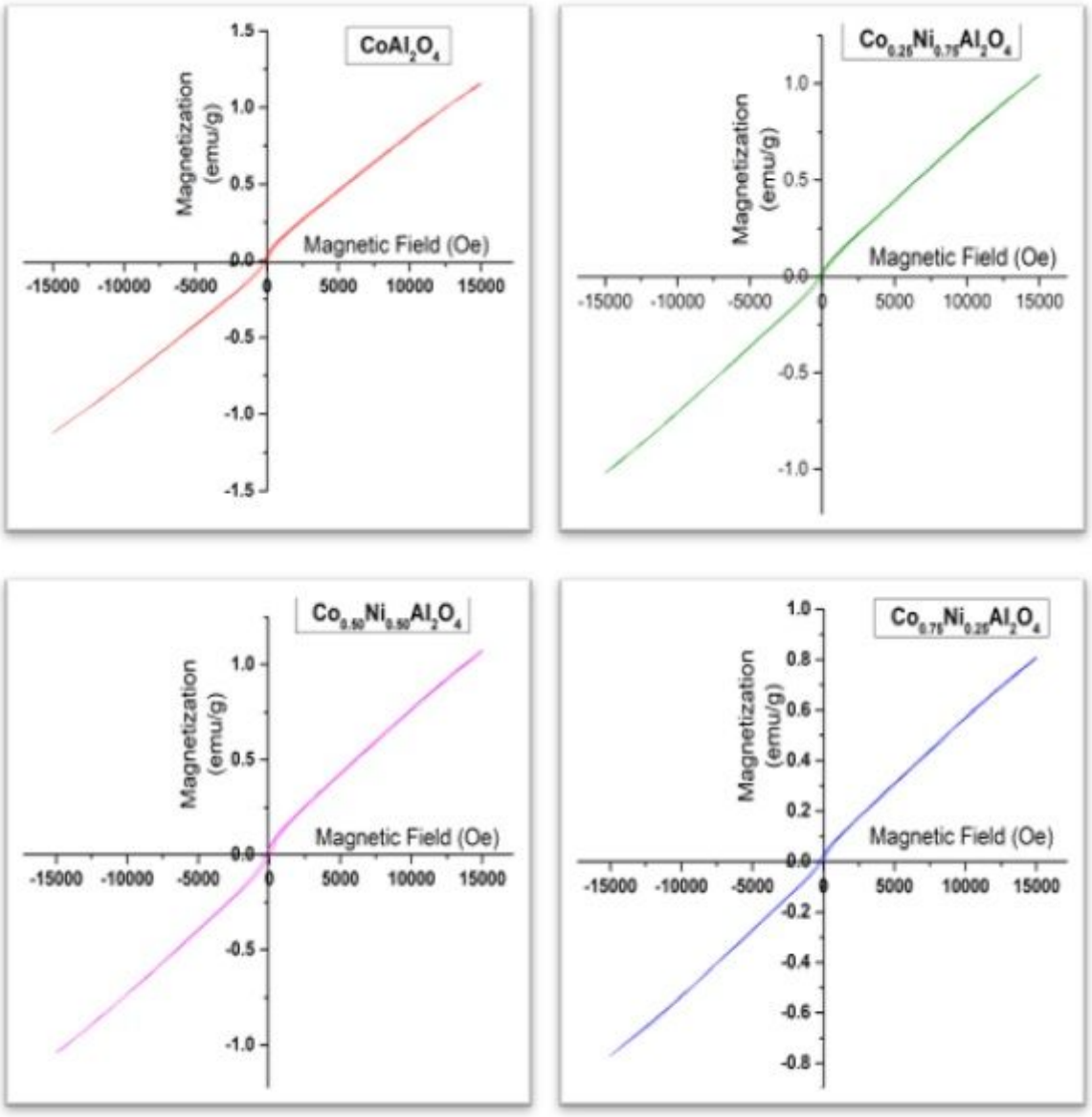

Figure 5

Hysteresis loops obtained for Co1-XNiXAl2O4 nanoparticles

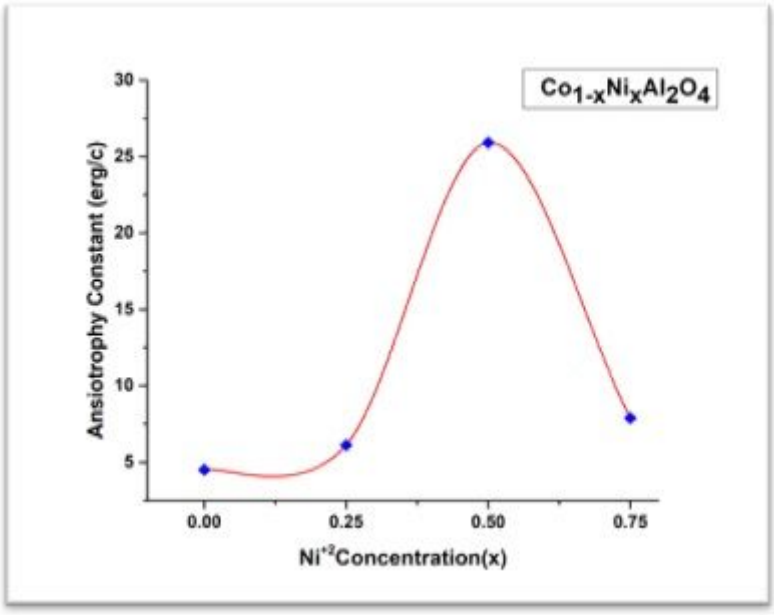

Figure 6

Variation of anisotropy constant ‘K’ with Ni concentration

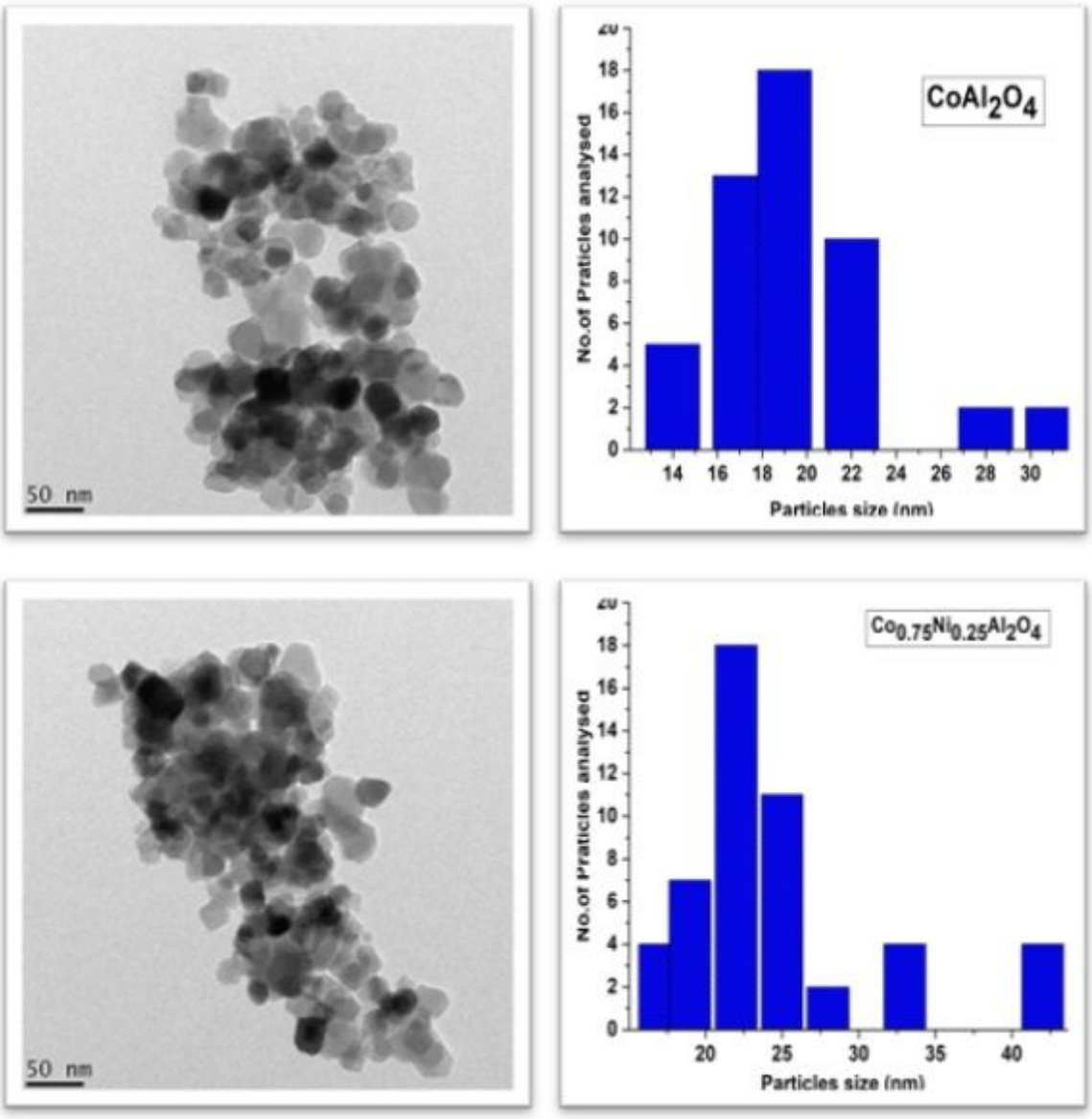

Figure 7

Transmission electron micrographs and particle size distribution histograms of CoAl2O4 and Co0.25Ni0.75Al2O4

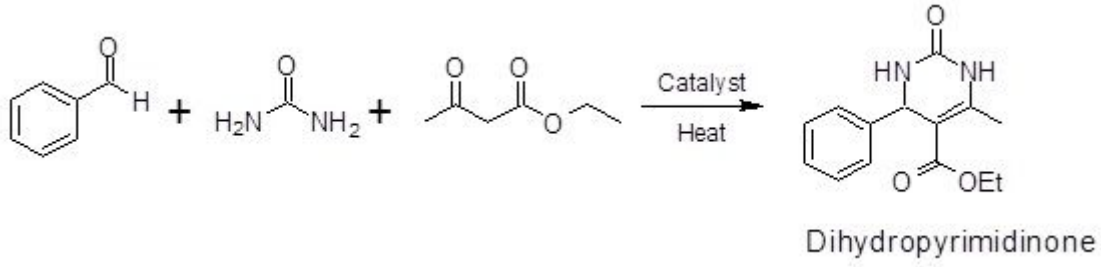

Figure 8

Bignelli reaction as a model catalytic application

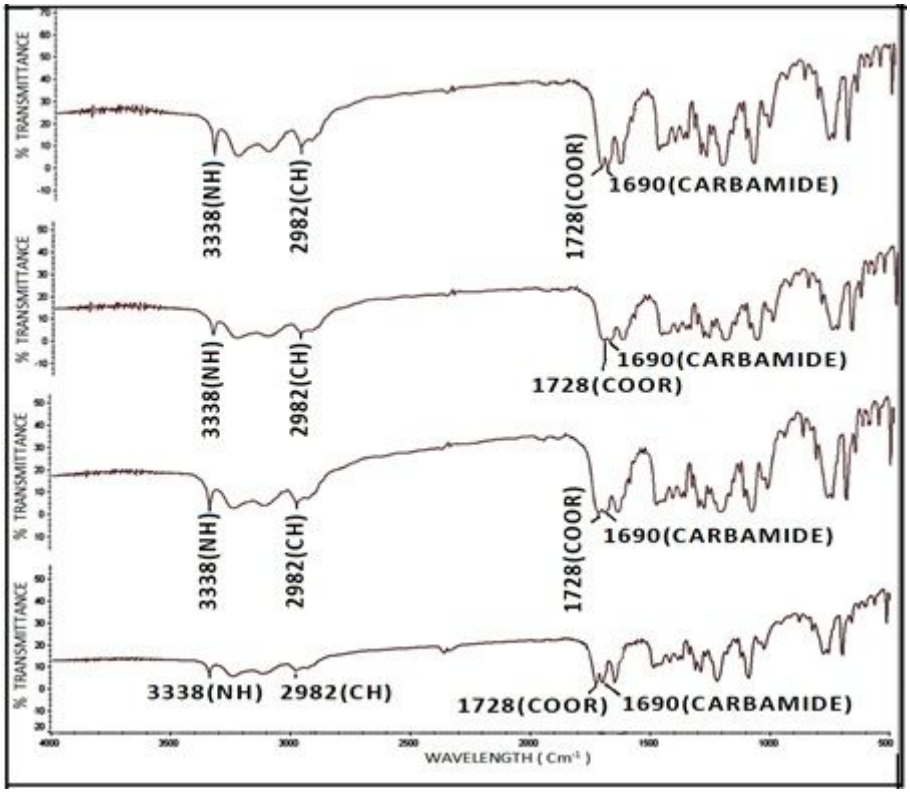

Figure 9

FTIR spectra of dihydropyrimidinone using Co1-XNiXAl2O4 nanocatalysts.

Supplementary Files

This is a list of supplementary files associated with this preprint. Click to download.

- Graphicalabstract.tif